Dynamic crack analysis in piezoelectric solids with non-linear crack-face boundary conditions by a time-domain BEM

M. Wünsche[1], Ch. Zhang[1], F. Garcia-Sanchez[2], A. Saez[3], J. Sladek[4] & V. Sladek[4]
[1]*Department of Civil Engineering, University of Siegen, Germany.*
[2]*Departamento de Ingeniería Civil, de Materiales y Fabricación, Universidad de Málaga, Spain.*
[3]*Departamento de Mecánica de Medios Continuos, Teoría de Estructuras e I. del Terreno, Universidad de Sevilla, Spain.*
[4]*Institute of Construction and Architecture, Slovak Academy of Sciences, Slovakia.*

Abstract

This paper presents a hypersingular time-domain boundary element method for transient dynamic crack analysis in two-dimensional (2-D), homogeneous and linear piezoelectric solids. Stationary cracks in infinite and finite piezoelectric solids under impact loading are considered. A combination of the strongly singular displacement boundary integral equations (BIEs) and the hypersingular traction BIEs is used in the present analysis. A Galerkin method is implemented for the spatial discretisation, while a collocation method is applied for the temporal discretisation. An explicit time-stepping scheme is obtained to compute the unknown boundary data, including the generalised crack-opening-displacements, numerically. An iterative solution algorithm is developed to consider the non-linear, semi-permeable electrical crack-face boundary condition. Furthermore, an additional iteration scheme for crack-face contact analysis is implemented at time-steps where physically meaningless crack-face intersection occurs. Numerical examples are presented and discussed


WIT Transactions on State of the Art in Science and Engineering, Vol 43, © 2010 WIT Press
www.witpress.com, ISSN 1755-8336 (on-line)
doi:10.2495/978-1-84564-492-5/25

to show the effects of the electrical crack-face boundary conditions on the dynamic intensity factors.

Keywords: Piezoelectric solids, Electrically permeable, impermeable and semi-permeable cracks, Dynamic crack analysis, Time-domain BEM, Dynamic intensity factors.

1 Introduction

Due to their inherent coupling effects between mechanical and electrical fields, piezoelectric materials are receiving increasing attention in modern technical applications such as smart devices and structures like transducers, actuators and sensors. Dynamic crack analysis in piezoelectric solids is of considerable importance to fracture and damage mechanics, design and optimisation as well as non-destructive material testing of piezoelectric structures. Since analytical solutions are available only for very simple crack geometries and loading conditions, efficient numerical methods are needed to solve general problems. Among many available numerical methods, the boundary element method (BEM) is very attractive for transient dynamic analysis of piezoelectric solids (e.g. [1–3]).

The formulation of the mechanical and the electrical boundary conditions on the crack-faces plays an important role in the crack analysis of piezoelectric materials. The mechanical boundary conditions are usually defined as traction-free or self-equilibrated stresses and, consequently, physically meaningless intersection of both crack-faces cannot appear. Besides the mechanical crack-face boundary conditions, several electrical crack-face boundary conditions are proposed in the literature. Since the electrical permittivity of a medium inside the crack is usually very small, the crack-face boundary condition is defined often as electrically impermeable. This model is mathematically exact for an electrical permittivity of zero. On the other side, the crack can be defined as electrically permeable, which is accurate for closed cracks or if the electrical permittivity is infinite. A more realistic non-linear crack-face boundary condition was introduced by Hao and Shen [4], where a limited electrical permittivity (electrically semi-permeable) of a medium inside the crack is considered. Several iterative solution algorithms have been developed for static crack analysis using the FEM [5–9] and the BEM [10] to take into account this semi-permeable crack-face boundary condition. Generally more complicated and of advanced technical interest is the dynamic analysis of electrically semi-permeable cracks, since additional transient effects induced by the dynamic loading and the scattered wave fields may influence the behaviour of the dynamic intensity factors (IFs) significantly. Dynamic crack analysis of electrically semi-permeable cracks using the FEM has been presented by Enderlein et al. [11].

In this paper, the initial-boundary value problem of transient dynamic crack analysis in piezoelectric solids is formulated and a hypersingular time-domain

BEM is developed. The cracked piezoelectric solid is subjected either to an electrical impact, or a mechanical impact, or a combination of both electrical and mechanical impact loadings. A combination of the strongly singular displacement boundary integral equations (BIEs) and the hypersingular traction BIEs is used. To solve the time-domain BIEs numerically, the temporal discretisation is performed by a collocation method, while the spatial discretisation is carried out by a Galerkin method. 2-D time-domain piezoelectric fundamental solutions [12] are implemented in the present time-domain BEM. To describe the local behaviour of the generalised crack-opening-displacements (CODs) at the crack-tips correctly, crack-tip elements are applied near the crack-tips. Time integration is performed analytically and special analytical techniques are developed to evaluate the strongly singular and the hypersingular boundary integrals. An explicit time-stepping scheme is used to compute the unknown CODs and the dynamic IFs. For electrically semi-permeable cracks, an iterative solution procedure is developed. An additional iterative solution procedure for crack-face contact analysis is implemented to avoid a physically meaningless intersection of both crack-faces. To show the effects of the electrical crack-face boundary conditions on the dynamic IFs, numerical examples are presented and discussed.

2 Problem statement

We consider a 2D, homogeneous, generally anisotropic and linear piezoelectric solid with a crack of arbitrary shape as shown in Figure 1.

In the absence of body forces and electrical charges, and using the quasi-electrostatic assumption, the cracked solid satisfies the generalised equations of motion

$$\sigma_{iJ,i}(\mathbf{x},t) = \rho\delta^*_{JK}\ddot{u}_K(\mathbf{x},t), \quad \delta^*_{JK} = \begin{cases} \delta_{JK}, & J,K = 1,2 \\ 0, & otherwise \end{cases}, \tag{1}$$

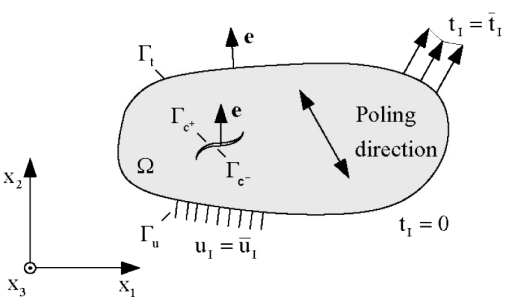

Figure 1: A cracked piezoelectric solid.

and the generalised constitutive equations

$$\sigma_{iJ}(\mathbf{x},t) = C_{iJKl}u_{K,l}(\mathbf{x},t), \tag{2}$$

where ρ is the mass density, δ^*_{JK} is the generalised Kronecker delta and u_I represents the generalised displacements

$$u_I = \begin{cases} u_i, & I = 1,2 \\ \varphi, & I = 4 \end{cases} \tag{3}$$

in which u_i and φ are the displacements and the electrical potential. Furthermore, σ_{iJ} are the generalised stresses

$$\sigma_{iJ} = \begin{cases} \sigma_{ij}, & J = 1,2 \\ D_i, & J = 4 \end{cases} \tag{4}$$

with σ_{ij} and D_i being the stresses and the electric displacements, and C_{iJKl} denotes the generalised elasticity tensor

$$C_{iJKl} = \begin{cases} c_{ijkl}, & J,K = 1,2 \\ e_{lij}, & J = 1,2, \quad K = 4 \\ e_{ikl}, & J = 4, \quad K = 1,2 \\ -\varepsilon_{il}, & J,K = 4 \end{cases}. \tag{5}$$

In eqn (5), c_{ijkl} is the elasticity tensor, e_{ijk} is the piezoelectric tensor and ε_{il} is the dielectric permittivity.

Throughout the analysis, a comma after a quantity designates spatial derivatives, while superscript dots stand for temporal derivatives of the quantity. Lower case Latin indices take the values 1 and 2 (elastic), while capital Latin indices take the values 1, 2 (elastic) and 4 (electric). Unless otherwise stated, the conventional summation rule over repeated indices is implied.

Taking into account the notation of eqns (3)–(5), the cracked solid Ω satisfies the initial conditions

$$u_I(\mathbf{x},t) = \dot{u}_I(\mathbf{x},t) = 0 \quad \text{for } t \le 0 \tag{6}$$

and the boundary conditions

$$t_I(\mathbf{x},t) = \overline{t}_I(\mathbf{x},t), \quad \mathbf{x} \in \Gamma_t, \tag{7}$$

$$u_I(\mathbf{x},t) = \overline{u}_I(\mathbf{x},t), \quad \mathbf{x} \in \Gamma_u, \tag{8}$$

with t_I being the generalised traction vector defined by

$$t_I(\mathbf{x},t) = \sigma_{jI}(\mathbf{x},t) \quad e_j(\mathbf{x}). \tag{9}$$

In eqns (7)–(9), e_j is the outward unit normal vector, Γ_t is the external boundary where the generalised tractions t_I are prescribed and Γ_u is the external boundary where the generalised displacements u_I are given. On the upper and the lower crack-face Γ_{c^+} and Γ_{c^-} self-equilibrated generalised tractions are considered. In order to avoid a physically meaningless material interpenetration between both crack-faces, the following constraint condition is introduced on the crack:

$$\Delta u_2(\mathbf{x} \in \Gamma_{c^+}, t) \geq 0, \tag{10}$$

where $\Delta u_2(\mathbf{x},t)$ is the normal component of the generalised CODs defined by

$$\Delta u_I(\mathbf{x},t) = u_I(\mathbf{x} \in \Gamma_{c^+}, t) - u_I(\mathbf{x} \in \Gamma_{c^-}, t). \tag{11}$$

Besides the mechanical crack-face boundary conditions, three different electrical crack-face boundary conditions are applied. The impermeable electrical crack-face boundary condition

$$D_i(\mathbf{x} \in \Gamma_{c^+}, t) = D_i(\mathbf{x} \in \Gamma_{c^-}, t) = 0 \tag{12}$$

means that both crack-faces are physically free of electrical displacements. In contrast, the permeable electrical crack-face boundary condition

$$D_i(\mathbf{x} \in \Gamma_{c^+}, t) = D_i(\mathbf{x} \in \Gamma_{c^-}, t),\ \varphi(\mathbf{x} \in \Gamma_{c^+}, t) - \varphi(\mathbf{x} \in \Gamma_{c^-}, t) = 0 \tag{13}$$

implies identical potentials at both crack-faces. For semi-permeable cracks, the boundary conditions are

$$D_i(\mathbf{x} \in \Gamma_{c^+}, t) = D_i(\mathbf{x} \in \Gamma_{c^-}, t), \quad \mathrm{D_i}(\mathbf{x} \in \Gamma_{c^+}, \mathrm{t}) = -\kappa_c \frac{\varphi(\mathbf{x} \in \Gamma_{c^+}, \mathrm{t}) - \varphi(\mathbf{x} \in \Gamma_{c^-}, \mathrm{t})}{\mathrm{u_i}(\mathbf{x} \in \Gamma_{c^+}, \mathrm{t}) - \mathrm{u_i}(\mathbf{x} \in \Gamma_{c^-}, \mathrm{t})} \tag{14}$$

where both opposite crack-faces are considered as a set of corresponding parallel capacitors and κ_c is the electrical permittivity inside the crack.

3 Time-domain BIEs and fundamental solutions

In the present paper, the initial-boundary value problem is solved by a time-domain BEM. In the sense of a weighted residual formulation in space, the time-domain Galerkin BIEs are defined by

$$\begin{aligned} \int_{\Gamma_b} \psi(\mathbf{x}) u_J(\mathbf{x},t) \mathrm{d}\Gamma_x = {} & \int_{\Gamma_b} \psi(\mathbf{x}) \int_{\Gamma_b} \left[u_{IJ}^G(\mathbf{x},\mathbf{y},t) * t_I(\mathbf{y},t) - t_{IJ}^G(\mathbf{x},\mathbf{y},t) * u_I(\mathbf{y},t) \right] \mathrm{d}\Gamma_y \mathrm{d}\Gamma_x \\ & + \int_{\Gamma_b} \psi(\mathbf{x}) \int_{\Gamma_{c^+}} t_{IJ}^G(\mathbf{x},\mathbf{y},t) * \Delta u_I(\mathbf{y},t)\ \ \mathrm{d}\Gamma_y \mathrm{d}\Gamma_x, \end{aligned} \tag{15}$$

where $u_{IJ}^G(x,y,t)$ and $t_{IJ}^G(x,y,t)$ are the displacement and the traction fundamental solutions. Furthermore, $\Gamma_b = \Gamma_u + \Gamma_t$ and an asterisk '*' denotes the

Riemann convolution which is defined by

$$g(\mathbf{x},t) * h(\mathbf{x},t) = \int_0^t g(\mathbf{x},t-\tau)h(\mathbf{x},\tau)\mathrm{d}\tau. \tag{16}$$

The traction fundamental solutions $t_{IJ}^G(x,y,t)$ are obtained by the substitution of the displacement fundamental solutions into the constitutive eqn (2) as

$$t_{IJ}^G(\mathbf{x},\mathbf{y},t) = C_{qIKr}e_q(\mathbf{y})u_{KJ,r}^G(\mathbf{x},\mathbf{y},t). \tag{17}$$

The time-domain traction BIEs are derived by substituting eqn (15) into eqns (2) and (9). Taking into account the boundary conditions (7) and (8), the resulting BIEs are applied on the upper crack-face Γ_{c+} to yield a complete set of equations for the displacements and the tractions on Γ_b and the CODs on Γ_c

$$\begin{aligned}\int_{\Gamma_{c^+}} \psi(\mathbf{x})\ \ t_J(\mathbf{x},t)\mathrm{d}\Gamma_x &= \int_{\Gamma_{c^+}} \psi(\mathbf{x})\int_{\Gamma_b}\left[v_{IJ}^G(\mathbf{x},\mathbf{y},t) * t_I(\mathbf{y},t) - w_{IJ}^G(\mathbf{x},\mathbf{y},t) * u_I(\mathbf{y},t)\right]\mathrm{d}\Gamma_y\mathrm{d}\Gamma_x\partial x \\ &+ \int_{\Gamma_{c^+}} \psi(\mathbf{x})\int_{\Gamma_{c^+}} w_{IJ}^G(\mathbf{x},\mathbf{y},t) * \Delta u_I(\mathbf{y},t)\mathrm{d}\Gamma_y\mathrm{d}\Gamma_x,\end{aligned} \tag{18}$$

where $v_{IJ}^G(x,y,t)$ and $w_{IJ}^G(x,y,t)$ are the traction and the higher-order traction fundamental solutions, which are defined by

$$v_{IJ}^G(\mathbf{x},\mathbf{y},t) = -C_{pIKs}e_p(\mathbf{x})u_{KJ,s}^G(\mathbf{x},\mathbf{y},t), \tag{19}$$

$$w_{IJ}^G(\mathbf{x},\mathbf{y},t) = -C_{pIKs}e_p(\mathbf{x})C_{qJLr}e_q\quad(\mathbf{y})u_{KL,sr}^G(\mathbf{x},\mathbf{y},t). \tag{20}$$

The displacement Galerkin-BIEs (15) are applied to the external boundary of the cracked solid, while the traction Galerkin-BIEs (18) are used on the crack-faces in the present time-domain BEM. The weighting function $\psi(\mathbf{x})$ is chosen as the spatial shape function employed for the interpolation of the boundary values. It should be mentioned that the displacement BIEs (15) are strongly singular, while the tractions BIEs (18) involve a hypersingularity at $\mathbf{x}=\mathbf{y}$.

The time-domain dynamic fundamental solutions for homogeneous, anisotropic and linear piezoelectric solids are not available in explicit forms. Here, the fundamental solutions derived by Wang and Zhang [12] using the Radon transform technique are implemented. They can be expressed in the 2-D case by a line-integral over a unit circle as

$$u_{IJ}^G(\mathbf{x},\mathbf{y},t) = \frac{H(t)}{4\pi^2}\int_{|\mathbf{n}|=1}\sum_{m=1}^{M}\frac{P_{IJ}^m}{\rho c_m}\frac{1}{c_m t + \mathbf{n}\cdot(\mathbf{y}-\mathbf{x})}\mathrm{d}\mathbf{n}, \tag{21}$$

where $H(t)$, $\mathbf{n}$, c_m and P_{IJ}^m denote the Heaviside step function, the wave propagation vector, the phase velocities of the elastic waves and the projection operator, respectively [12]. Integrating eqn (21) by parts with respect to the time

and applying the properties of convolution integrals, the time-domain fundamental solutions can be divided into a singular static plus a regular dynamic part as

$$u_{IJ}^{G}(\mathbf{x},\mathbf{y},t) * f(t) = u_{IJ}^{S}(\mathbf{x},\mathbf{y}) \quad f(t) + u_{IJ}^{R}(\mathbf{x},\mathbf{y},t) * \dot{f}(t), \tag{22}$$

where the superscripts S and R stand for the static and the dynamic parts, respectively. The singular static part can be reduced to an explicit expression while the regular dynamic part can be given only as a line-integral over a unit circle.

4 Numerical solution procedure

To solve the strongly singular displacement BIEs (15) and the hypersingular traction BIEs (18), a Galerkin method is applied for the spatial discretisation [3]. The external boundary and the crack-faces are discretised by linear elements. At the crack-tips, square-root shape-functions are used to describe the local behaviour of the generalised CODs properly. This ensures an accurate and direct calculation of the dynamic IFs from the numerically computed generalised CODs. Strongly singular and hypersingular boundary integrals are computed analytically by special techniques [3,13]. The temporal discretisation is performed by a collocation method. By using linear temporal shape-functions, time integrations can also be performed analytically. The line-integrals over a unit circle arising in the dynamic fundamental solutions are computed numerically by using standard Gaussian quadrature formula.

After temporal and spatial discretisations and invoking the initial conditions and boundary conditions, the following time-stepping scheme can be obtained

$$\mathbf{x}^{K} = (\mathbf{C}^{1})^{-1}\left[\mathbf{D}^{1} \quad \mathbf{y}^{K} + \sum_{k=1}^{K-1}(\mathbf{B}^{K-k+1} \quad \mathbf{t}^{k} - \mathbf{A}^{K-k+1} \quad \mathbf{u}^{k})\right] \tag{23}$$

in which $\mathbf{x}^{K}$ represents the vector with the unknown boundary data, while $\mathbf{y}^{K}$ denotes the vector with the prescribed boundary data. Eqn (23) is an explicit time-stepping scheme for computing the unknown boundary data, including the generalised CODs time-step by time-step.

An efficient solution for non-linear crack-face boundary conditions is one of the significant advantages of the BEM since the generalised tractions and displacements are primary variables in the BIEs. In the investigated initial-boundary value problem, there are two different non-linear crack-face boundary conditions. At time-step where a crack-face intersection occurs, an iterative crack-face contact analysis [14,15] is performed to take into account eqn (10) in the numerical algorithm. Furthermore, an additional iterative solution procedure is developed to solve the non-linear semi-permeable electrical crack-face boundary condition (14) at time-step where the crack is open.

5 Numerical examples

In this section, numerical examples are presented and discussed to show the effects of the different crack-face boundary conditions on the dynamic IFs. For convenience, the following normalised dynamic IFs [3] are introduced

$$K_{\mathrm{I}}^{*}(t)=\frac{K_{\mathrm{I}}(t)}{K_0},\ K_{\mathrm{II}}^{*}(t)=\frac{K_{\mathrm{II}}(t)}{K_0},\ K_{\mathrm{IV}}^{*}(t)=\frac{e_{22}}{\varepsilon_{22}}\frac{K_{\mathrm{IV}}(t)}{K_0},\ K_0=\sigma_0\sqrt{\pi a}. \quad (24)$$

To measure the intensity of the electrical impact, the following loading parameter is introduced

$$\chi=\frac{e_{22}}{\varepsilon_{22}}\frac{D_0}{\sigma_0}, \quad (25)$$

where σ_0 and D_0 are the loading amplitudes.

5.1 A crack in an infinite piezoelectric plate under an impact tensile loading

In the first example, as shown in Figure 2, a finite crack of length $2a$ in an infinite and linear piezoelectric solid subjected to an impact tensile loading $\sigma(t)=\sigma_0 H(t)$ is investigated, where $H(t)$ denotes the Heaviside step function and σ_0 is the loading amplitude.

As piezoelectric material $BaTiO_3$ is chosen, which has the material constants

$$\begin{aligned} &C_{11}=150.0\,\mathrm{GPa},\ C_{12}=146.0\,\mathrm{GPa},\ C_{22}=44.0\,\mathrm{GPa},\ C_{66}=66.0\,\mathrm{GPa},\\ &e_{21}=-4.35\,\mathrm{C/m^2},\ e_{22}=17.5\,\mathrm{C/m^2},\ e_{16}=11.4\,\mathrm{C/m^2},\\ &\varepsilon_{11}=9.87\,\mathrm{C/(GVm)},\ \varepsilon_{22}=11.2\,\mathrm{C/(GVm)}. \end{aligned} \quad (26)$$

and the mass density $\rho = 5{,}800\ \mathrm{kg/m^3}$. The crack is divided into 20 elements and a normalised time-step of $c_L\Delta t/a = 0.05$ is used. Plain strain condition is

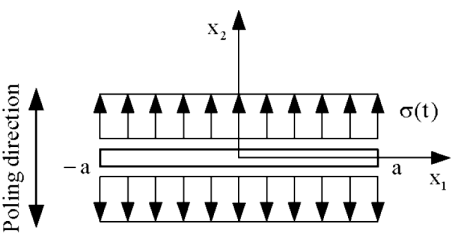

Figure 2: A crack in an infinite linear piezoelectric plate under an impact loading.

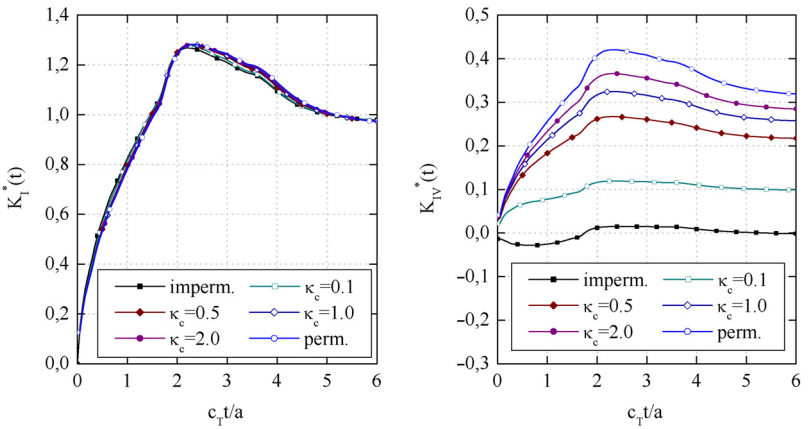

Figure 3: Normalised dynamic IFs for different electrical permittivity κ_c.

assumed in the numerical calculations. A comparison of the normalised dynamic IFs obtained by the present time-domain BEM using different electrical crack-face boundary conditions given in eqns (12)–(14) is presented in Figure 3.

The normalised mode-I dynamic IFs are very similar without a significant difference for all investigated electrical crack-face boundary conditions and permittivities κ_c. Since no shear stress components are induced by the investigated loading, poling direction is normal to the crack-face and a transversal isotropic material behaviour occurs and the mode-II dynamic IF vanishes. In contrast to the mode-I IFs, the electrical permittivity κ_c has a significant influence on the normalised mode-IV dynamic Ifs, which can be clearly seen in Figure 3. For a permeable crack, the non-existence of the crack in the electrical field results in the curve of the mode-IV IF, which has a similar behaviour as that for mode-I. In contrast, the impermeable crack-face boundary condition leads to the strongest electrical crack-tip field and therefore the mode-IV IF depends only weakly on the time. As well expected, the results of the semi-permeable cracks are between the bounds given by the impermeable and permeable electrical crack-face boundary conditions.

5.2 A central crack in a rectangular piezoelectric plate

In the second example, we consider a homogeneous and linear piezoelectric rectangular plate containing a central crack of length $2a$, as shown in Figure 4. The cracked plate is subjected to a combined impact tensile loading $\sigma(t)=\sigma_0 H(t)$ and impact electrical loading $D(t)=D_0 H(t)$. The geometrical data $h = 20.0$ mm, $2w=h$ and $2a = 4.8$ mm are assumed in the numerical

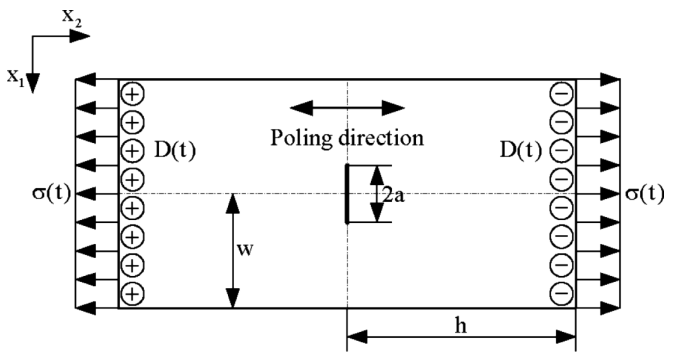

Figure 4: A piezoelectric plate with a central crack subjected to impact loading.

calculations. The piezoelectric material PZT-5H with the mass density ρ = 7,500 kg/m^3 and the material constants

$$C_{11} = 126.0\,\text{GPa},\ C_{12} = 84.1\,\text{GPa},\ C_{22} = 117.0\,\text{GPa},$$
$$C_{66} = 23.0\,\text{GPa},\ e_{21} = -6.5\,\text{C/m}^2,\ e_{22} = 23.3\,\text{C/m}^2,\ e_{16} = 17.0\,\text{C/m}^2 \quad (27)$$
$$\varepsilon_{11} = 15.04\,\text{C/(GVm)},\ \varepsilon_{22} = 13.0\,\text{C/(GVm)}$$

is considered. The external boundary is divided into uniformly distributed elements with the length of 1.0 mm and the crack is discretised by 12 elements. A normalised time-step of $c_L\Delta t/h = 0.04$ is chosen and plane strain condition is assumed. A comparison of the numerical results obtained by the present time-domain BEM and the FEM using ANSYS for $\chi = 1$ and electrical impermeable and permeable crack-face boundary conditions, given in eqns (12) and (13), are shown in Figure 5. The computations are performed with and without the consideration of the crack-face contact. The element type PLANE223 is used in the FEM calculations. Quarter-point elements are implemented to describe the local $r^{1/2}$-behaviour of the generalised CODs at the crack-tips properly. The dynamic IFs are computed directly by the generalised CODs as in the time-domain BEM.

The normalised mode-I and mode-IV dynamic IFs of the present time-domain BEM and ANSYS show a very good agreement. The mode-II dynamic IF vanishes, since no shear stress components are induced by the investigated loading and transversally isotropic material behaviour. Since a combined electrical and mechanical impact loading is applied, the normalised dynamic IFs start from a non-zero value due to the quasi-electrostatic assumption for the electrical field. This implies that the cracked plate is immediately subjected to the electrical impact. It can be clearly seen that the investigated electrical impact loading leads to a physically meaningless

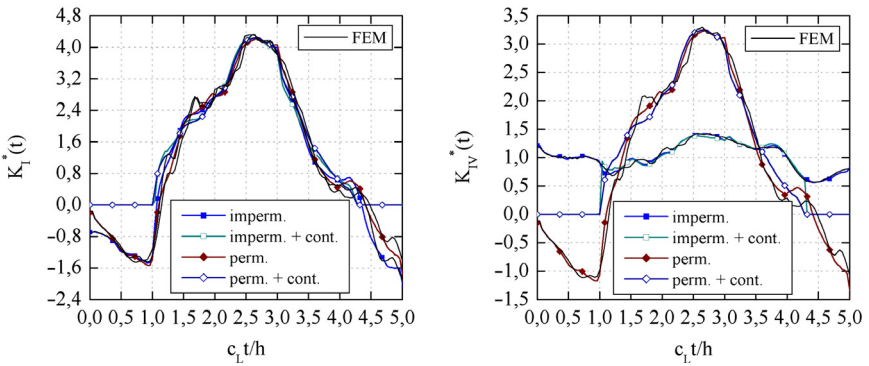

Figure 5: Comparison of the normalised dynamic IFs for different crack-face boundary conditions.

material interpenetration from $c_L t/h = 0$ until $c_L t/h = 1.1$ and therefore a crack-face contact analysis is required in this time interval. It should be mentioned that the computation is without friction because the slip component $\Delta u_1(t)$ of the CODs is zero. The elastic waves induced by the impact tensile loading reach the crack-tips near $c_L t/h = 1.0$ and thereafter the dynamic IFs increase rapidly until their maximum peaks.

To illustrate the influence of the electrical permittivity κ_c on the dynamic Ifs, several computations have been carried out using semi-permeable electrical crack-face boundary condition (14) and contact conditions (10). The numerical results of the present time-domain BEM for a combined dynamic loading $\chi = 1$ are presented in Figure 6. To point out the influence of the scattered wave fields on the dynamic IFs, the corresponding static results are given in Table 1.

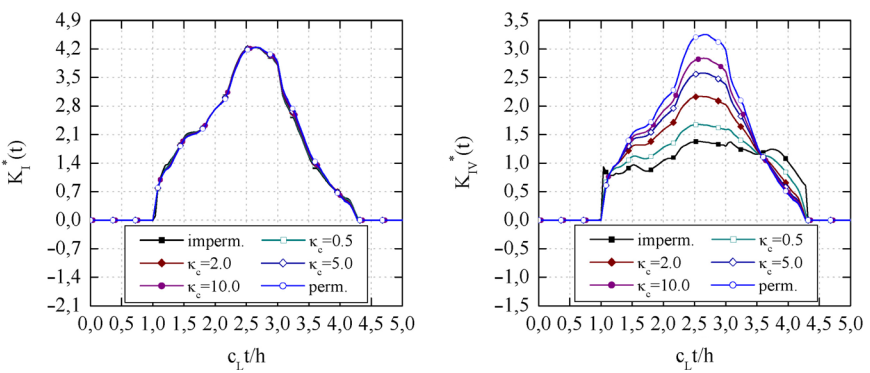

Figure 6: Normalised dynamic IFs for different electrical permittivity κ_c.

Table 1: Normalised static IFs for different electrical permittivity κ_c.

κ_c	K_{I}^{*}	K_{II}^{*}	K_{IV}^{*}
0.0 (imperm.)	1.05	0.00	1.05
0.5	1.05	0.00	0.95
2.0	1.05	0.00	0.87
5.0	1.05	0.00	0.84
10.0	1.05	0.00	0.82
∞ (perm.)	1.05	0.00	0.81

As in the previous example, a variation of the electrical permittivity κ_c has a significant influence on the normalised static and dynamic mode-IV IFs. The difference between the mode-IV IFs for permeable and impermeable crack-face boundary conditions is more pronounced for dynamic loading, which is induced by the scattered wave fields. According to the geometry of the cracked plate and the applied loading, the dynamic IFs for both crack-tips are identical.

6 Conclusions

This paper presents a hypersingular time-domain BEM for 2-D transient dynamic crack analysis in homogenous and linear piezoelectric solids with non-linear mechanical and electrical boundary conditions. A Galerkin method is used for the spatial discretisation while a collocation method is adopted for the temporal discretisation. The dynamic time-domain fundamental solutions for homogenous, anisotropic and linear piezoelectric solids are implemented. The spatial discretisation is performed with linear elements away from the crack-tips. Adjacent to the crack-tips, square-root elements are implemented which ensures a direct and accurate calculation of the dynamic IFs from the numerically computed generalised CODs. In contrast, a collocation method using linear shape function is applied for the temporal discretisation. With the exception of the line-integrals over a unit circle arising in the time-domain fundamental solutions, the temporal and the spatial integrations can be performed analytically. This feature makes the present time-domain BEM particularly attractive and efficient. After temporal and spatial discretisation, an explicit time-stepping scheme is obtained for computing the unknown boundary data including the CODs. An iterative solution algorithm is developed to handle the non-linear semi-permeable electrical crack-face boundary condition. In order to avoid the possible crack-face contact, a second iterative solution procedure is implemented. Numerical examples are presented and discussed to investigate the influences of the electrical and the mechanical impact loadings, different electrical crack-face boundary conditions and the

crack-face contact on the dynamic IFs. The obtained numerical results show a good agreement with those of the FEM and a significant influence of the electrical permeability on the mode-IV dynamic IF.

Acknowledgement

This work was supported by German Research Foundation (DFG, Project Nos. ZH 15/6-1 and ZH 15/6-3). The financial support is gratefully acknowledged.

References

[1] García-Sánchez, F., Zhang Ch. & Sáez, A., 2-D transient dynamic analysis of cracked piezoelectric solids by a time domain BEM. *Computer Methods in Applied Mechanics and Engineering*, **197**, pp. 3108–3121, 2008.
[2] Gaul, L., Kögl, M. & Wagner, M., *Boundary Element Methods for Engineers and Scientists*, Springer-Verlag: Berlin, Heidelberg, 2003.
[3] Wünsche, M., García-Sánchez, F., Sáez, A. & Zhang, Ch., A 2D time-domain collocation-Galerkin BEM for dynamic crack analysis in piezoelectric solids. *Engineering Analysis with Boundary Elements*, **34**, pp. 377–387, 2010.
[4] Hao, T.H. & Shen, Z.Y., A new electric boundary condition of electric fracture mechanics and its applications. *Engineering Fracture Mechanics*, **47,** pp. 793–802, 1994.
[5] Grübener, O., Kamlah, M. & Munz, D., Finite element analysis of cracks in piezoelectric materials taking into account the permittivity of the crack medium. *Engineering Fracture Mechanics*, **70**, pp. 1399–1413, 2003.
[6] Kemmer, G., Computation of electro-mechanical intensity parameters for cracks in piezo-ceramics. Ph.D. Thesis, TU Dresden, Germany, 2000 (in German).
[7] Landis, C.M., Energetically consistent boundary conditions for electro-mechanical fracture. *International Journal of Solids and Structures*, **41**, pp. 6291–6315, 2004.
[8] McMeeking, R.M., Crack tip energy release rate for a piezoelectric compact tension specimen. *Engineering Fracture Mechanics*, **64**, pp. 217–244, 1999.
[9] Wippler, K., Ricoeur, A. & Kuna, M., Towards the computation of electrically permeable cracks in piezoelectrics. *Engineering Fracture Mechanics*, **71**, pp. 2567–2587, 2004.
[10] Denda, M., BEM analysis of semipermeable piezoelectric cracks. *Key Engineering Materials*, **383**, pp. 67–84, 2008.
[11] Enderlein, M., Ricoeur, A. & Kuna, M., Finite element techniques for dynamic crack analysis in piezoelectrics. *International Journal of Fracture*, **134**, pp. 191–208, 2005.

[12] Wang, C.-Y. & Zhang, Ch., 3-D and 2-D dynamic Green's functions and time-domain BIEs for piezoelectric solids. *Engineering Analysis with Boundary Elements*, **29**, pp. 454–465, 2005.
[13] Gray, L.J., Evaluation of singular and hypersingular Galerkin boundary integrals: direct limits and symbolic computation. *Advances in Boundary Elements*, ed. V. Sladek & J. Sladek, Computational Mechanics Publishers: Southampton, UK, pp. 33–84, 1998.
[14] Aliabadi, M.H., *The Boundary Element Method Volume 2, Applications in Solids and Structures*, Computational Mechanics Publications: John Wiley & Sons, 2002.
[15] Phan, A.-V., Napier, J.A.L., Gray, L.J. & Kaplan, T., Symmetric-Galerkin BEM simulation of fracture with frictional contact. *International Journal for Numerical Methods in Engineering*, **57**, pp. 835–851, 2003.